Original Paper

Quantitative investigation of nanofluid imbibition in tight oil reservoirs based on NMR technique

Tian-Tian Zhang [a, b], Zhi-Ping Li [a, b, **], Caspar Daniel Adenutsi [c], Yong-Zhou Wei [d], Zhen-Fu Ma [e], Qing You [a, b, *]

[a] School of Energy Resources, China University of Geosciences, Beijing, 10083, China
[b] Beijing Key Laboratory of Unconventional Natural Gas Geological Evaluation and Development Engineering, Beijing, 10083, China
[c] Core and Rock Properties Laboratory, Department of Petroleum Engineering, Faculty of Civil and Geo-Engineering, Kwame Nkrumah University of Science and Technology, Kumasi, Ghana
[d] Binnan Oil Production Plant, Shengli Oilfield Company, SINOPEC, Binzhou, 256606, Shandong, China
[e] Hekou Oil Production Plant, Shengli Oilfield Company, SINOPEC, Dongying, 257200, Shandong, China

ARTICLE INFO

ABSTRACT

Nanofluids have been effective chemical additives for enhanced oil recovery (EOR) in tight oil reservoirs due to their special properties. However, oil imbibition recoveries vary for different nanofluids. The oil/water distribution in rocks during imbibition using various nanofluids was less discussed in previous studies. In this study, we systematically examined the imbibition efficiencies of various nanofluids at 60 °C. Furthermore, the migration of nanofluids and oil distribution in the rock pores were monitored using nuclear magnetic resonance (NMR). The nanofluids were prepared by dispersing silica nanoparticles and five different types of surfactants (i.e., anionic-nonionic, anionic, nonionic, amphoteric and cationic surfactants in deionized (DI) water. Subsequently, interfacial tension (IFT) and contact angle measurements were conducted to reveal the underlying EOR mechanisms of various nanofluids. The experimental results showed that the EOR potential of the different types of nanofluids was in the order anionic-nonionic > anionic > nonionic > amphoteric > cationic > brine. Anionic-nonionic (sodium lauryl ether sulfate (SLES)) and anionic (sodium dodecyl sulfonate (SDS)) nanofluids exhibited excellent capability of wettability alteration, and increased oil recovery by 27.96% and 23.08%, respectively, compared to brine. The NMR results also showed that mesopores (0.1—1 μm) were the dominant developed pores in the rocks, and contributed the most to imbibition efficiency. In addition, the imbibition of nanofluids initially took place in mesopores and micropores before moving into macropores. This study provides fundamental information on the selection of nanofluids for EOR in tight oil reservoirs. The study also improved the understanding of oil/water distribution during the imbibition of the proposed nanofluids.

1. Introduction

Nanofluids, which refer to fluids prepared by dispersing nanoscale materials in a liquid medium (Li Z. et al., 2018b; Liang et al., 2021a; Wang Z. et al., 2021b), have been intensively investigated in diverse fields of study such as heat energy (Qiu et al., 2019; Zadeh et al., 2020), biomedicine (Xu et al., 2021b; Zhang C. et al., 2021a), and chemical engineering (Wuebbeler et al., 2021) due to their significant influences on interfacial properties. Besides, nanoparticles also possess large specific surface area and high surface energy, which can effectively solve the arduous problems associated with hydrocarbon recovery from tight or ultralow permeable reservoirs during oilfield development (Kuang et al., 2018; Adenutsi et al., 2019; Afekare et al., 2020). Nanofluids have gained considerable attention in enhanced oil recovery as potential fluids that are applied to improve interfacial activity and regulate wettability (Mousavi et al., 2021; Sangeetha et al., 2021; Hassan et al., 2022).

* Corresponding author.
** Corresponding author. School of Energy Resources, China University of Geosciences, Beijing, 10083, China.
E-mail addresses: lzp_cugb@163.com (Z.-P. Li), youqing@cugb.edu.cn (Q. You).

Nanofluids exhibit a greater ability to reduce interfacial tension and alter wettability than their base fluids (Zhang T. et al., 2021b; Afra et al., 2021; Liang et al., 2021b; Jafarbeigi et al., 2021). Li Y. et al. (2018a) synthesized a novel silica-based nanofluid, and verified the interfacial activity of functional nanoparticles by interfacial tension and interfacial dilational modulus measurements. They reported that the developed active nanoparticles can effectively reduce the interfacial tension (IFT) and alter the surface wettability compared to silica nanoparticles, resulting in exceptional oil displacement. Kuang et al. (2018) investigated the synergistic effect of various nanofluids on the interfacial properties of oil/brine/rock systems, and found that nanofluids were able to modify interfacial tension and alter wettability of rock surfaces. This enhanced oil imbibition efficiency significantly in Berea sandstone rock samples. The authors also pointed out that the co-adsorption of nanoaggregates and surfactant molecules at the rock interface were responsible for wettability alteration. Sagala et al. (2020) examined the influence of nanopyroxene on interfacial tension and wettability, and then probed the oil efficacies of nanofluids as EOR agents. Core flooding experiments showed that nanopyroxene-based nanofluid improved oil recovery by an additional 12%–14.5% after water flooding. Additionally, they believed nanopyroxene was a promising additive for EOR applications.

Nuclear magnetic resonance (NMR) technique is a non-destructive method which is widely applied in the petroleum and natural gas industry to characterize pore structure and fluid distribution in porous media (Sun et al., 2020; Chen et al., 2021; Zhao et al., 2022). Xu et al. (2022) quantitatively assessed the imbibition of fracturing fluid and influencing factors by dynamic simulation experiments and NMR technique. They indicated that micropores were the best contributors to oil imbibition recovery for fracturing fluid, and also reported that the imbibition effect of the hydrophilic rock was better than that of the lipophilic rock. Mao et al. (2020) employed porosity data derived from low-field NMR to characterize the wetting of coal pores. They suggested that macropores were more readily wetted by aqueous liquid than mesopores, and the degree of water wetting of the macropores had a stronger negative effect on coal flotation than that of the mesopores. Wang F. et al. (2021a) analyzed the pore fractal characteristics of a sandstone reservoir using NMR and rate-controlled porosimetry. By considering the movable fluid distribution, the authors proposed a novel NMR method. They found out that the fractal dimensions of pores occupied with fully movable, partially movable and immovable fluids had a strong correlation with petrophysical properties of the tight sandstone reservoir. Su et al. (2018) employed NMR technology to test the wettability of shale. The authors also compared the abundance of organic matter, movable hydrocarbon content, clay content and carbonate content of shale samples with different wetting characteristics. They concluded that the existence of organic matter was responsible for the oil wettability of shale porosity. However, research on the spontaneous imbibition of nanofluids in tight oil rocks using NMR technology is scarce. Therefore, careful investigations of NMR tests are necessary to evaluate spontaneous imbibition using various nanofluids in tight oil reservoirs.

In the following subsections, the materials used in this study and preparation of various functional nanofluids are initially introduced. Then, the effects of functional nanofluids on IFT and wettability are discussed in detail. Afterwards, the migration trends of nanofluids in sandstone cores during spontaneous imbibition using NMR technique are discussed. Observations of spontaneous imbibition characteristics such as NMR porosity, wettability and oil distribution in sandstone rocks are reported. Additionally, the results of using effective porosity fractal dimension to evaluate nanofluids on movable fluids during imbibition is discussed.

Finally, the effect of nanofluids on oil imbibition efficacies are investigated, and the underlying mechanisms involved in EOR using nanofluids are explained.

2. Materials and methods

2.1. Materials

In this work, hydrophilic silica sol with purity of 40 wt% was used. The diameter of silica nanoparticles was approximately 10 nm. Five chemical agents including dodecyl trimethyl ammonium bromide (DTAB, 98 wt%), lauramidopropyl hydroxy sulfobetaine (LHSB, 35 wt%), C12 alkyl glucoside (APG12, 50 wt%), sodium dodecyl sulfonate (SDS, 98 wt%), and sodium lauryl ether sulfate (SLES, 70 wt%) were used as modifiers. For comparison purposes, the selected chemical agents all contain twelve carbon chains. Crude oil used for spontaneous imbibition was obtained from the Changqing Oilfield, which had a density of 0.8183 g/cm^3 and a viscosity of 3.15 mPa s at 60 °C. The same oil was also used in IFT and contact angle (CA) measurements. 3 wt% NaCl solution was utilized as the reservoir brine.

The core samples were obtained from the Changqing tight sandstone reservoir. SEM micrographs of rock samples are shown in Fig. 1. The target sandstone reservoir was rich in quartz, with a distribution range of 30%–70%. All core samples were approximately 25 mm in diameter and 35 mm in length. These core plugs were cleaned and then dried at 105 °C for at least 2 days, to ensure the rocks were completely dry (Li Y. et al., 2018a). The permeabilities and porosities of these dried core samples were in the ranges of 0.072–0.088 mD and 9.73–11.26%, respectively.

2.2. Nanofluid preparation

Five types of nanofluids were prepared by dispersing 0.05 wt% silica sol in deionized (DI) water with or without 0.1 wt% chemical agents (i.e., cationic, amphoteric, nonionic, anionic-nonionic, and anionic surfactants). The preparation of functionalized nanofluid is shown in Fig. 2. To better improve the dispersion of silica nanoparticles in DI water, the mixtures were ultrasonicated for 20 min by a JY92-IIN ultrasonic homogenizer at 60 °C so as to obtain the transparent active nanofluids. The properties of the nanofluids are listed in Table 1. In this work, 'SiO$_2$ nanofluid' refers to solution of silica nanoparticles without chemical agents.

2.3. Interfacial tension and contact angle measurements

Interfacial tension measurements between nanofluids and crude oil were performed using the automatic pendant drop method with a TRACKER interfacial rheometer (TECLIS, France) at 60 °C. In this method, an oil droplet was introduced into the nanofluid in a quartz cuvette through a U-shaped motor driven syringe. Then, the IFT data was recorded as the oil droplet stabilized (Fig. 3(a)). The measurements were repeated in triplicates for each sample, and the standard error was within ±5%. The details of the experimental setup are provided in the work of Jiang et al. (2016). Notably, to ensure the accuracy of the IFT measurements, the system required noiseless environment during the measurements.

The contact angles of nanofluid/crude oil/rock systems were determined using the captive bubble method with a JC2000D1 contact angle measuring instrument (Shanghai) at 60 °C (Fig. 3(b)) (Liu et al., 2019; Xu et al., 2021a). Prior to the tests, the glass slides were aged in paraffin for 48 h at 60 °C to obtain oil-wet surfaces (Li Y. et al., 2018a). The measurement procedure is as follows: (1) The quartz chamber was thoroughly cleaned before any measurements. (2) The aged oil-wet glass slide was put on a crystal holder
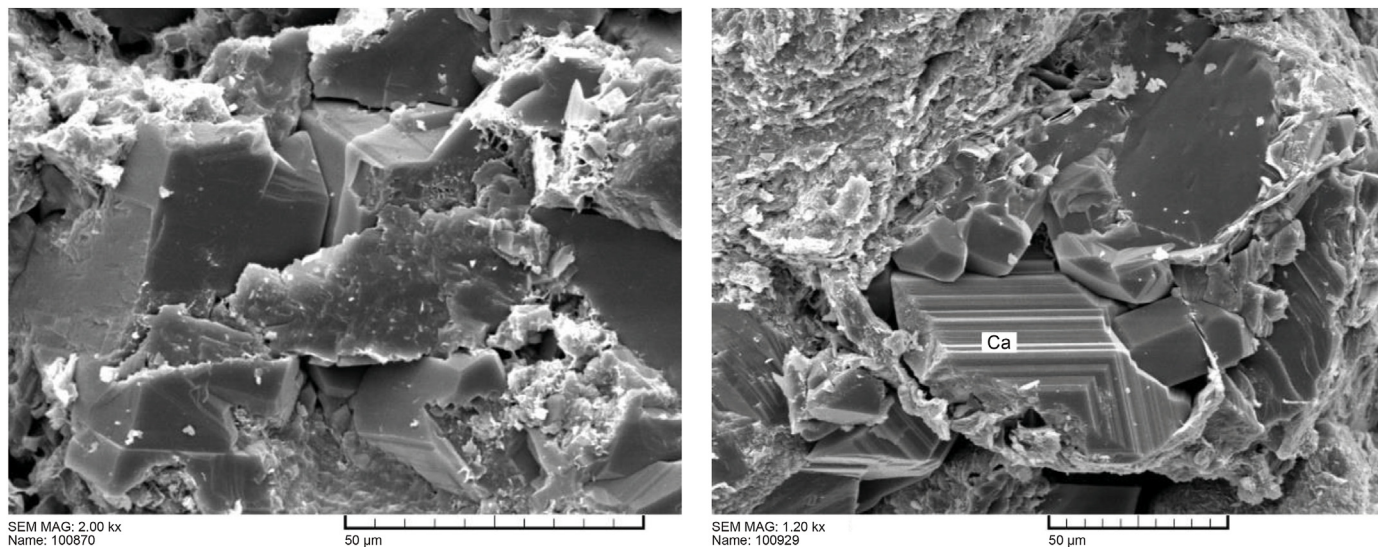
Fig. 1. SEM micrographs of the rock sample obtained from the Changqing sandstone reservoir.
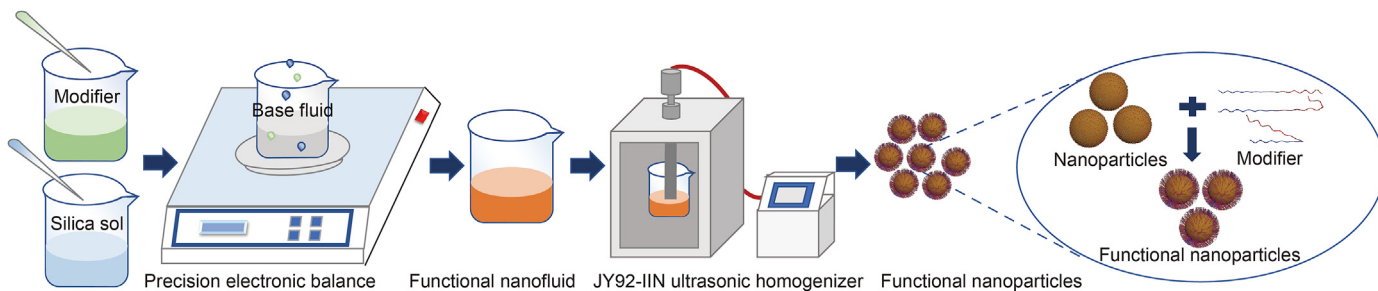

Fig. 2. Schematic illustration of synthesis of functionalized silica nanoparticles.

Table 1
Nanofluid properties.

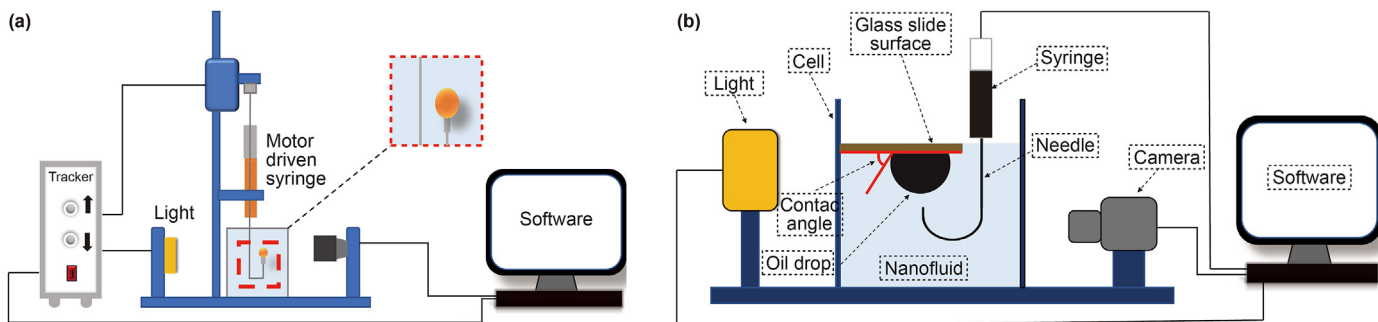| Nanofluid	Nanoparticle	Nanoparticle concentration, wt%	Surfactant	Surfactant type	Surfactant concentration, wt%	Particle size, nm
SiO$_2$	SiO$_2$	0.05	/	/	/	10.39
SiO$_2$ + DTAB	SiO$_2$	0.05	DTAB	Cationic	0.1	18.46
SiO$_2$ + LHSB	SiO$_2$	0.05	LHSB	Amphoteric	0.1	17.73
SiO$_2$ + APG12	SiO$_2$	0.05	APG12	Nonionic	0.1	16.84
SiO$_2$ + SDS	SiO$_2$	0.05	SDS	Anionic	0.1	15.56
SiO$_2$ + SLES	SiO$_2$	0.05	SLES	Anionic-nonionic	0.1	11.62

Fig. 3. Schematic diagrams of (**a**) interfacial tension and (**b**) contact angle measurement devices.

in the quartz chamber, and nanofluid was then gradually injected. (3) An oil droplet on the oil-wet substrate of glass slide was created using an inverted needle. (4) When the submerged glass slide reached an equilibrium state after 24 h, the images of oil droplets were taken by a high-resolution microscopic camera, and then the static contact angles before and after immersion of nanofluid were measured by software. (5) To obtain the dynamic contact angles, the glass slides were kept in nanofluid for 24 h. The changes in oil contact angles with time were observed and measured for 24 h. The measurements were repeated three times to ensure the reliability of the contact angle results. The measurements had an accuracy of ±2°.

2.4. Spontaneous imbibition tests and NMR measurements

Spontaneous imbibition tests were conducted using a series of different types of nanofluids to evaluate oil displacement effects. Rock core samples with similar permeabilities and porosities were selected for spontaneous imbibition tests using the procedure reported in the study of Zhou et al. (2019). This is reported as follows: (1) The preserved core samples were fully saturated with crude oil from the Changqing Oilfield, and the T_2 spectra of the oil-saturated core samples were measured. (2) All rock samples were placed in Amott cells with nanofluids or brine at 60 °C. During the imbibition process, the displaced oil floated on the surface of the water, and the corresponding amount of oil extracted versus time was recorded. It is worth mentioning that the oil-saturated rocks needed to be immersed in crude oil for 24 h at 60 °C in advance so as to avoid the effect of oil expansion in core pores. In addition, the fluids used for spontaneous imbibition were also preheated to 60 °C. (3) Subsequently, the core samples were taken out at regular intervals, and the corresponding T_2 spectra were measured during the imbibition. (4) Step 3 was repeated until the completion of imbibition tests. To avoid the mutual interference of hydrogen signals between oil and water, deuterium oxide (D_2O) without magnetic moment was employed to prepare nanofluids and brine.

2.5. NMR fractal theory

NMR is an effective and nondestructive technology widely used for monitoring fluid distributions in pores and to determine the pore size distribution (PSD) of sandstone rocks (Mao et al., 2020; Wang Z. et al., 2021b; Xu et al., 2021; Liu et al., 2021). The number of hydrogen atoms present within a fluid in a porous medium can be detected through the transverse relaxation time (T_2), and thus the pore structure of the reservoir can be described. The total NMR T_2 can be expressed as follows (Yuan et al., 2019):

$$\frac{1}{T_2} = \frac{1}{T_{2B}} + \rho\left(\frac{S}{V}\right) + \frac{A(\gamma GT_E)^2}{12} \tag{1}$$

where T_2 is the transverse relaxation, ms; T_{2B} is the volume (free) relaxation time of fluid, ms; S is the pore surface area, cm²; V is the pore volume, cm³; ρ is the transverse surface relaxation strength of rocks, μm/ms; A is the diffusion coefficient, μm²/ms; G is the magnetic field gradient, 10^{-4} T/cm; T_E is the echo spacing, ms; γ is the gyromagnetic ratio, $(T\ s)^{-1}$.

When there is only one type of fluid in the pores, the volume relaxation is much slower than the surface relaxation, so $1/T_{2B}$ can be ignored. In addition, when the magnetic field is uniform (the corresponding magnetic field gradient G is very low) and the echo interval (T_E) is short enough, the third diffusion coefficient term can also be ignored. Thus, Eq. (1) can be simplified as:

$$\frac{1}{T_2} = \rho\left(\frac{S}{V}\right) \tag{2}$$

The relationship between T_2 and pore diameter (d) can be expressed as:

$$\frac{1}{T_2} = \rho\left(\frac{S}{V}\right) = F_S\frac{\rho}{d} \tag{3}$$

$$d = CT_2 \tag{4}$$

where d is the pore diameter, nm; C is the conversion coefficient, ms/μm; F_S is the geometry factor. For spherical pores, $F_S = 3$; for cylindrical pores, $F_S = 2$.

Based on fractal geometry theory, the number (N) of pores larger than r conforms to the following power function (Li Y. et al., 2018a; Yuan et al., 2019; Chen et al., 2021):

$$N(>r) = \int_r^{r_{max}} S(r)dr = \alpha r^D \tag{5}$$

where $N(>r)$ is the number of pores of radii $> r$; r_{max} is the maximum pore radii, μm; $S(r)$ is the density function of pore size distribution; α is a fractal factor; and D represents the fractal dimension.

The cumulative volume fraction of pores with radii less than r can be described as (Chen et al., 2021):

$$S_v = \frac{r^{3-D} - r_{min}^{3-D}}{r_{max}^{3-D} - r_{min}^{3-D}} \tag{6}$$

Considering $r_{min} \ll r_{max}$, S_v can be expressed as:

$$S_v = \left(\frac{r}{r_{max}}\right)^{3-D} \tag{7}$$

Combining Eq. (3) and Eq. (7), Eq. (8) can be obtained as follows:

$$S_v = \left(\frac{T_2}{T_{2max}}\right)^{3-D} \tag{8}$$

Taking the logarithm of both sides of Eq. (8) can be expressed as:

$$\lg(S_v) = (3-D)\lg(T_2) + (D-3)\lg T_{2max} \tag{9}$$

If the pores have fractal characteristics, Eq. (7) will have a linear relationship. The fractal dimension D can be obtained by the slope (λ) as follows:

$$D = 3 - \lambda \tag{10}$$

3. Results and discussion

3.1. Characterization of functional silica nanoparticles

The dispersion stability of nanofluid is significant for oil displacement applications. However, silica nanoparticles usually aggregate and settle when dispersed in a suspension and this often renders the nanoparticles unsuitable for EOR applications (Chaturvedi and Sharma, 2020; Shalbafan et al., 2019; Zhou et al., 2020; Zhang et al., 2022). Therefore, it is necessary to systematically examine the stability of nanofluids. Fig. 4 presents the microstructure and morphology of silica nanoparticles and functional silica nanoparticles by transmission electron microscopy
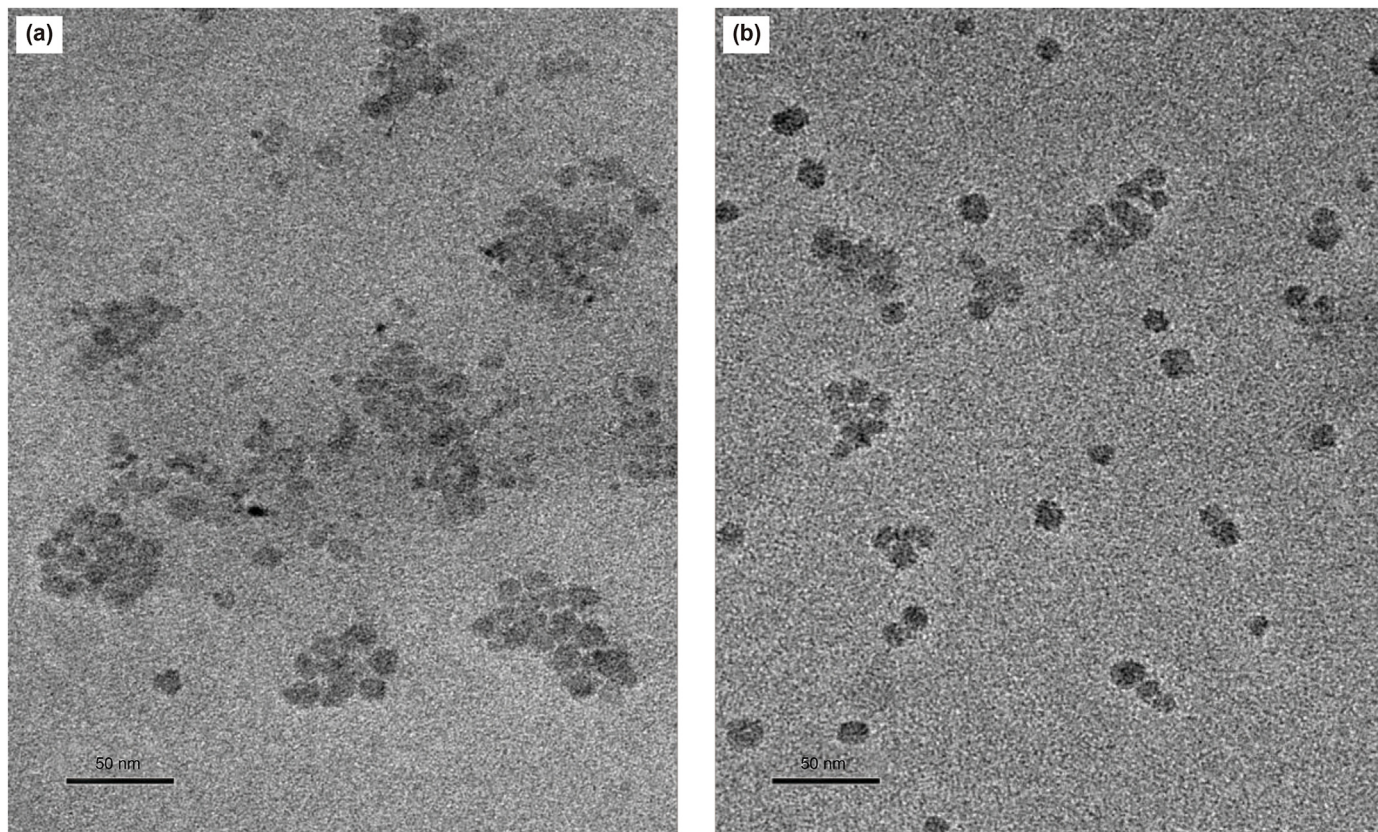
Fig. 4. TEM images of (**a**) silica nanoparticles and (**b**) functional silica nanoparticles (0.05 wt% SiO_2 + 0.1 wt% SLES) at 60 °C.

(TEM). Both nanoparticles generally displayed a spherical shape and were uniformly dispersed, and the according particle sizes were less than 20 nm, which was favorable for nanofluid flow in the tight porous medium. Visual observations revealed that functional silica nanoparticles exhibited better dispersibility than pure silica nanoparticles. The stability of silica nanoparticles at high temperature is of great significance to the practical applications of nanofluids in oil fields (Zhou et al., 2020). Thus, dynamic light scattering (DLS) and zeta potential measurement tests were conducted to characterize the stability of the nanofluids at 60 °C. It can be observed from Fig. 5 that the SiO_2 nanofluid was clear and
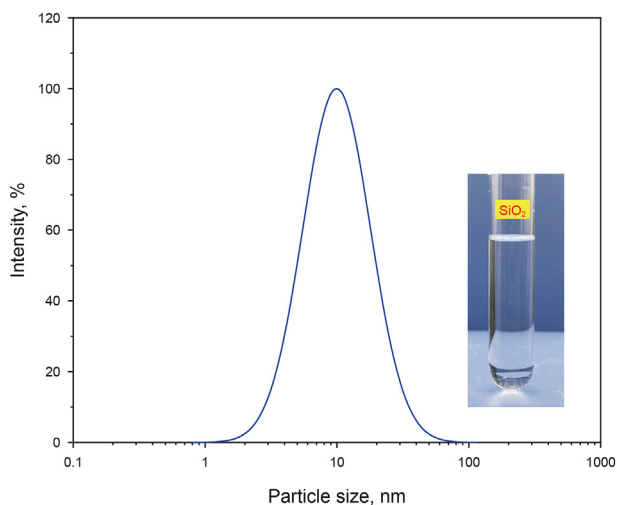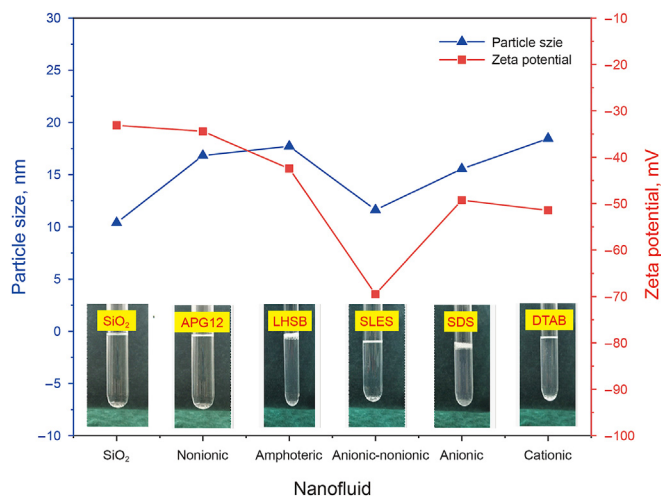

Fig. 6. Particle size and zeta potential results of various nanofluids (0.05 wt% SiO_2 + 0.1 wt% surfactants) at 60 °C.

transparent. The average size of the silica nanoparticles in DI water was 9.90 nm, which was in accordance with the results from TEM. The aforementioned five types of nanofluids were selected to analyze the dispersion stability. Fig. 6 plots particle size and zeta potential results for the various nanofluids at 60 °C. From Fig. 6, it was observed that no aggregation of silica nanoparticles occurred during the process of static settlement tests. In addition, the diameters of functional silica nanoparticles of various nanofluids ranged from 10 to 20 nm. The zeta potential (absolute value) of
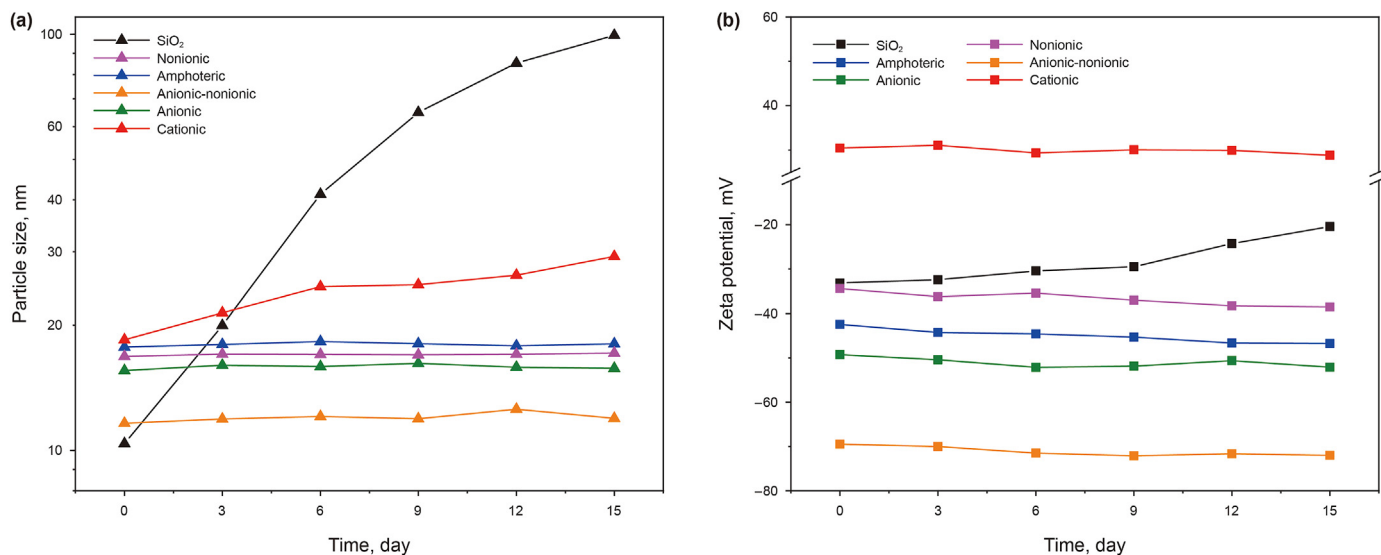

Fig. 5. Size distribution of silica nanoparticles in DI water at 60 °C.

Fig. 7. (**a**) Particle size and (**b**) zeta potential results of various nanofluids (0.05 wt% SiO$_2$ + 0.1 wt% surfactants) versus time at 60 °C.

nanofluids were in the range of 33.14–69.49 mV. It has been reported that an absolute value of zeta potential which is greater than 30 mV is sufficient to obtain stable nanofluids (Sentein et al., 2009). Furthermore, Fig. 7 plots the time dependence effect of various nanofluids on particle size and zeta potential. All proposed nanofluids were stored at 60 °C for 15 days. It was observed that the average particle size of pure silica nanofluid increased from 10.39 to 99.46 nm, and the absolute value of zeta potential decreased from 33.14 to 20.44 mV. However, the particle sizes and zeta potential of active nanofluids did not change significantly. In summary, pure silica nanofluid displayed poor stability at high temperatures, while the active nanofluids did not occur agglomeration. Nanofluids modified by different chemical agents in this work exhibited excellent dispersion stability, and could be stored for more than 15 days at 60 °C. Thus, the proposed nanofluids can be used for further studies in spontaneous imbibition.

3.2. Interfacial tension and contact angle

Nanofluids possess better performance in IFT reduction and wettability alteration as compared to simple surfactant solution, owing to their large specific surface area and high surface energy of nanoparticles (Kuang et al., 2018). To ascertain the effect of functional silica nanoparticles on the oil/water or oil/water/solid three-phase interface, the IFTs and contact angles were measured for the five stable nanofluids utilizing the rising bubble method (Maghzi et al., 2012). Fig. 8 illustrates the IFTs between crude oil and nanofluids modified by different types of surfactants at 60 °C. The oil-brine system without any additives was 27.44 mN/m. The interfacial tension of oil-SiO$_2$ nanofluid was 22.63 m/N, reflecting the less influence of pure silica nanoparticles on the interfacial properties. From Fig. 8, it was observed that the addition of pure surfactants or functional nanoparticles to DI water significantly decreased the oil-water interfacial tension, and the IFTs reached equilibrium state in a short time. During the IFT reduction process, a layer nanostructure was generated at the oil-water interface by SiO$_2$ nanoparticles. This adsorption behavior was similar to that of surfactants. This caused the SiO$_2$ nanoparticles to increase in their ability to reduce the oil-water interfacial tension (Li et al., 2017; Kuang et al., 2018). Additionally, the nanofluids made with nonionic, amphoteric and cationic surfactants displayed considerably lower IFTs than anionic and anionic-nonionic nanofluids. The

IFT results showed that the lower oil-water interfacial tension caused by the nanofluids can effectively increase oil mobility in porous media.

The ability of nanofluids to alter wettability is more effective than IFT reduction, and this plays a vital role in EOR applications (Kathel and Mohanty, 2018; Nowrouzi et al., 2019). According to previous studies, the adsorption behavior of nanofluids on the rock surface facilitated the wettability change as observed via contact angle measurements (Al-Anssari et al., 2016; Nwidee et al., 2017). Thus, in this work, the oil-wet glass slides were immersed in brine, SiO$_2$, DTAB, LHSB, APG, SDS, and SLES nanofluids at 60 °C for 24 h, respectively. After the glass slide surfaces were treated with the 0.05 wt% nanofluids, the static contact angles were measured and presented in Fig. 9(a). The initial contact angle of brine without any chemical agent was 28°, indicating the glass slide surface was lipophilic (Li Y., et al., 2018a). From Fig. 9(a), these functional nanofluids altered the wettability of glass surfaces toward more water-wet (103–155°) except for DTAB nanofluid. Especially, the presence of anionic or nonionic surfactant type caused more water wetness of the solid surfaces. The DTAB nanofluid displayed a considerable IFT reduction, while only a slight change was observed in contact angles (from 28° to 76°). We believed that the hydrophilic head of the cationic surfactant DTAB was adsorbed to the negatively charged oil-wet solid surface, owing to electrostatic attraction. In addition, the hydrophobic chain of the DTAB extended into the nanofluid, resulting in less water wetness of solid surface (Xu et al., 2021a).

To further explore the effect of time dependence of nanofluids on wettability alteration, the oil droplets were captured on the oil-wet substrates of glass slides and was subsequently immersed in the above-mentioned mixtures for 24 h. The dynamic contact angle results are presented in Fig. 9(b). At the first 4 h, a thin wedge film was formed and this was confined in the oil/nanofluid/glass slide three-phase region by disjoining pressure owing to the co-adsorption of nanoparticles and surfactant molecules at the oil-water interface (Fig. 10) (Kuang et al., 2018). This aided the oil droplets to gradually separate along the glass surface, and sharply increased the oil contact angles. With the accumulation of nanoparticles and surfactant molecules at the three-phase region, the wedge film was extended forward as indicated by the arrow in Fig. 10. Thus, the contact angles continued to increase. In the end, the contact angle remained almost unchanged when the system
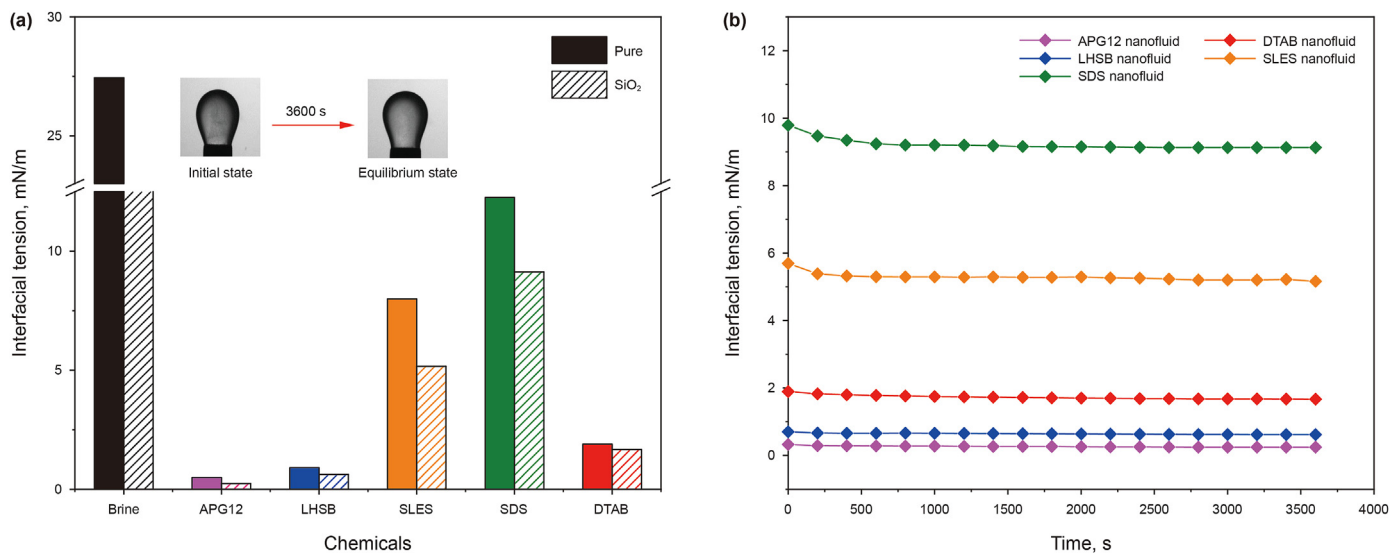
Fig. 8. (**a**) Equilibrium and (**b**) dynamic IFTs between nanofluids (0.05 wt% SiO_2 + 0.1 wt % surfactants in DI water) and crude oil at 60 °C.
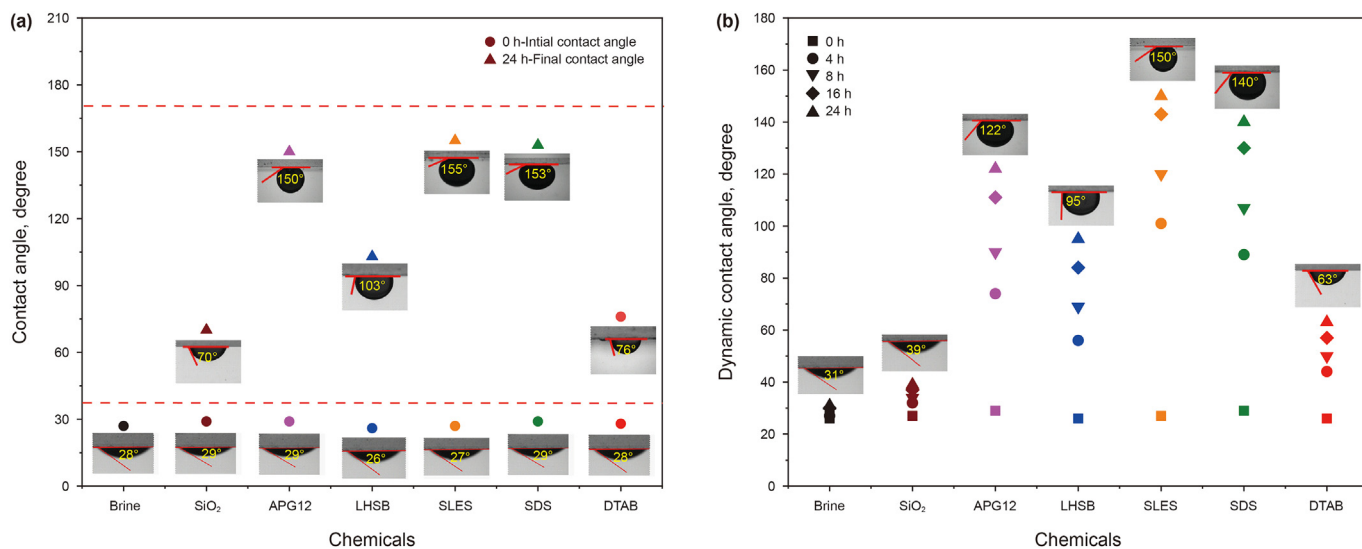

Fig. 9. (**a**) Static and (**b**) dynamic contact angles for nanofluids (0.05 wt% SiO_2 + 0.1 wt% surfactants in DI water)/crude oil/solid system at 60 °C.

stabilized (63−150°). The SLES nanofluid significantly changed the contact angle from 27° to 150°, while the DTAB nanofluid merely changed the contact angle from 28° to 63° compared to the brine and SiO_2 nanofluid. This behavior was expected because of the presence of electrostatic attraction between the positively self-assembled nanoparticles and the negatively charged glass slide.

Based on the above analysis, the coated nanoparticles led to more stable nanofluids and performed well in wettability alteration and oil displacement (Nwidee et al., 2017). Meanwhile, the wettability of the rock surface was irreversible (Liu et al., 2021). Thus, the selected nanofluids provided the essential foundation for further application in the following spontaneous imbibition tests.

3.3. NMR results

3.3.1. PSD analysis

NMR T_2 spectrum can effectively reflect the pore size distribution of the reservoir. The pore size is proportional to the T_2

relaxation time (Mao et al., 2020; Zhou et al., 2019). The longer the T_2 value, the larger the pore size of the sandstone core sample. Fig. 11 plots the T_2 spectrum curve and the HPMI pore size distribution in of the tight sandstone. The two plots were similar. Thus, Eq. (4) was utilized to convert the T_2 distribution into the PSD. From Fig. 11, it was observed that there were six points that coincided on the T_2 spectrum and HPMI plots. The parameters are listed in Table 2. The average conversion coefficient which was obtained through calculation was 0.10. Since the sandstone cores selected in this work had similar permeability (0.072−0.088 mD), the value of the conversion coefficient C was equal in these core samples. Thus, the PSDs can be obtained through NMR T_2 spectra, which provided a foundation for further study of the relation between oil recoveries and pore structure (Dai et al., 2019).

The distribution of the NMR T_2 spectrum of the sandstone core samples had a strong correlation with the pore size distribution, as listed in Table 3. The T_2 distributions and PSD of the seven oil saturated samples are plotted in Fig. 12(a and b). From Fig. 12(a), it
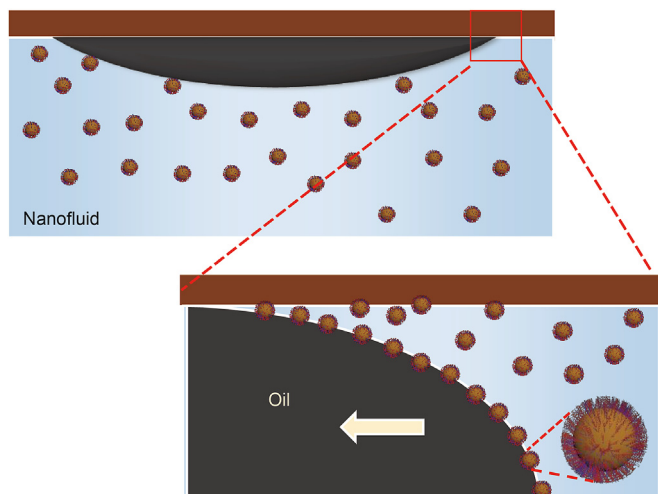
Fig. 10. Schematic illustration of oil displacement from a solid surface by functional nanofluid.
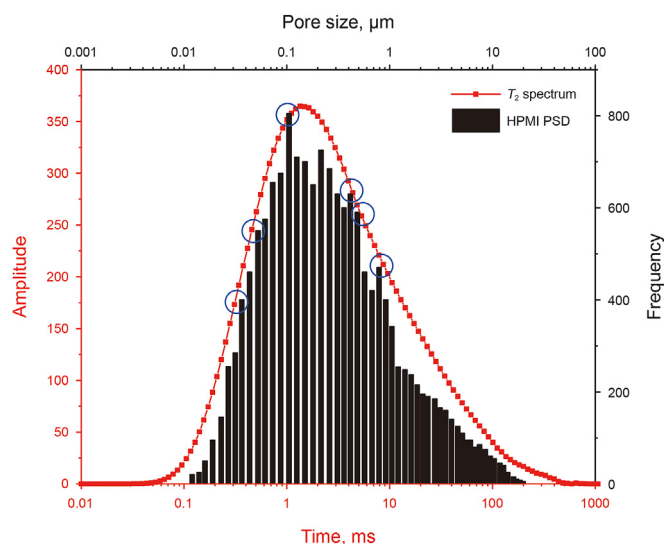

Fig. 11. The coupling relation between T_2 spectrum and HPMI curve.

Table 2
Results of the conversion coefficient C.

T_2, ms	D, μm	C, ms/μm
0.31	0.04	0.12
0.46	0.05	0.11
1.11	0.11	0.09
4.38	0.31	0.07
5.32	0.49	0.09
8.70	0.92	0.11

Table 3
Pore classification criteria for sandstone cores.

T_2, ms	Pore size, μm	Pore type
<1	<0.1	Micropore
1−10	0.1−1	Mesopore
>10	>1	Macropore

was observed that all NMR T_2 spectra of oil-saturated sandstone core samples were unimodal and ranged from 0.1 to 1000 ms. The dominant peaks appeared at relaxation times ranging from 1 to 3 ms. In addition, sandstone core pores can be divided into micropores (<0.1 μm), mesopores (0.1−1 μm) and macropores (>1 μm). Obviously, the proportion of mesopores was the highest, ranging from 50.54% to 52.12%, followed by micropores (26.88%−28.89%) and macropores (20.33%−21.65%). This implied that mesopores in the samples dominated micropores and macropores in the study area. These characteristics were consistent with the typical properties of the Changqing tight oil reservoir (Zhou et al., 2019).

3.3.2. Movable fluid distribution

NMR technique can intuitively and effectively detect the presence of fluid in rocks. The saturation and porosity of the movable fluid are essential indicators used to characterize the fluid flow capacity in the reservoir (Su et al., 2018). During the imbibition process, the movable fluid distribution can be obtained by subtracting the T_2 spectrum after imbibition from T_2 spectrum before imbibition. Fig. 13(a) plots the incremental and cumulative NMR T_2 porosity spectra of the cores that were immersed in 3 wt% brine and 0.05 wt% of various silica nanofluids, respectively. It was observed that the oil saturated cumulative porosity ranged from 10.70% to 11.26%, which was consistent with the results of the conventional petrophysical experiments (error range ±1.5%), as seen in Table 4. The cumulative porosity decreased to 6.74%−9.55% after imbibition with different fluids. This can be considered as the bound fluid porosity under imbibition conditions. The interval between the curves of oil saturated and post imbibition cumulative porosity was taken as the effective movable fluid porosity. Moreover, the NMR dominated peak values of all cores decreased, and the corresponding T_2 relaxation time became larger after imbibition. The difference in the T_2 relaxation time varied from 0.14 to 1.33 ms. Among the samples, core sample 6#, 7# had considerable changes before and after imbibition. This showed that the movable fluid in sample 6#, 7# was highly mobilized.

Fig. 13(b) shows the calculated movable fluid saturation, and Table 4 presents the petrophysical properties and NMR analysis results of the core samples. From Fig. 13(b) and Table 4, the movable fluid saturation was in the range of 11.39%−38.97%. In comparison with cores with various imbibition fluids, it was observed that less brine and pure nanofluid imbibed into samples 1# and 2#, and only a few drops of oil was produced during the imbibition process. While introducing the active nanoparticles modified by various surfactants to deionized water, the results demonstrated that the movable fluid of sample 7# adsorbed SLES nanofluid the most, followed by samples 5# and 6#, respectively. Meanwhile, sample 3# imbibed DTAB the least. This indicated that the movable fluid performance of core samples treated with these active nanofluids were better than that of the brine and pure nanofluid (Dai et al., 2019).

NMR fractal dimension can comprehensively characterize the complexity and heterogeneity of pore structure of the reservoir, which is an important bridge connecting the microscopic pore structure and macroscopic performance (Liu et al., 2021; Wang Z. et al., 2021b). Thus, careful investigations of the fractal characteristics of porous media in the sandstone core samples treated with various nanofluids are necessary, to further evaluate their effects on improving oil recovery. Fig. 14(a) plots the fractal dimension curve of the pores in the sandstone cores derived from Eq. (9). From the Fig. 14(a), it was observed that the overall fractal curve had a distinct inflection point at a T_2 value of 1.0 ms. The curves were divided into two sections, namely $T_2 > 1$ ms and $T_2 < 1$ ms, and the corresponding fractal dimension were assigned D_1 and D_2,
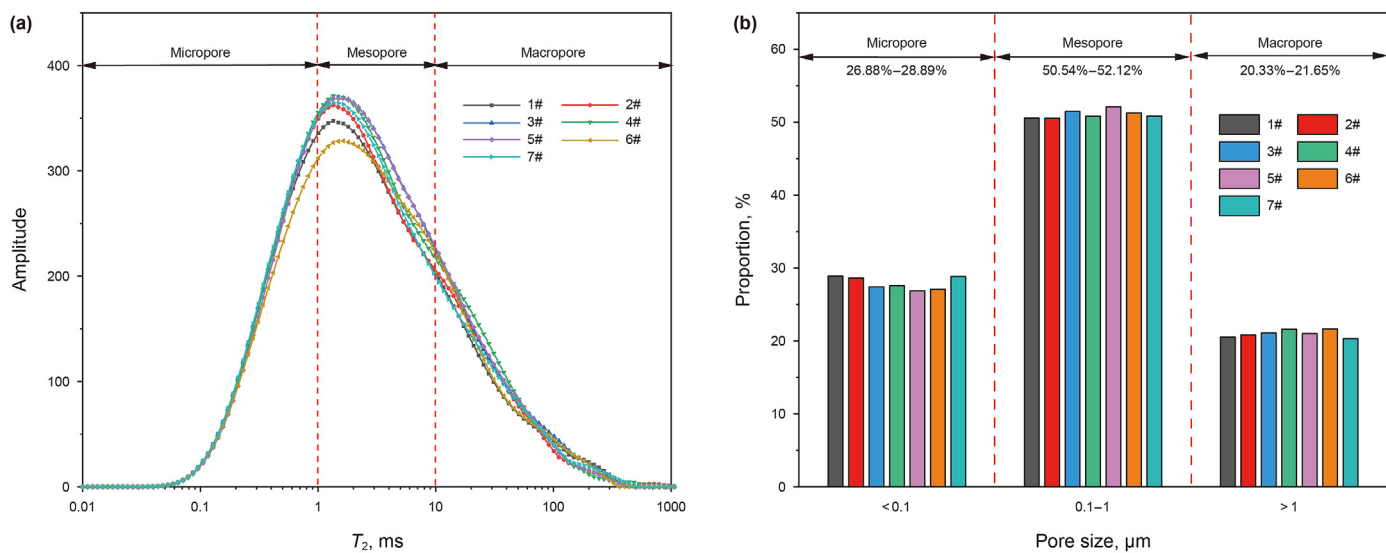
Fig. 12. (**a**) The T_2 relaxation distribution and (**b**) PSD of saturated oil sandstone cores.
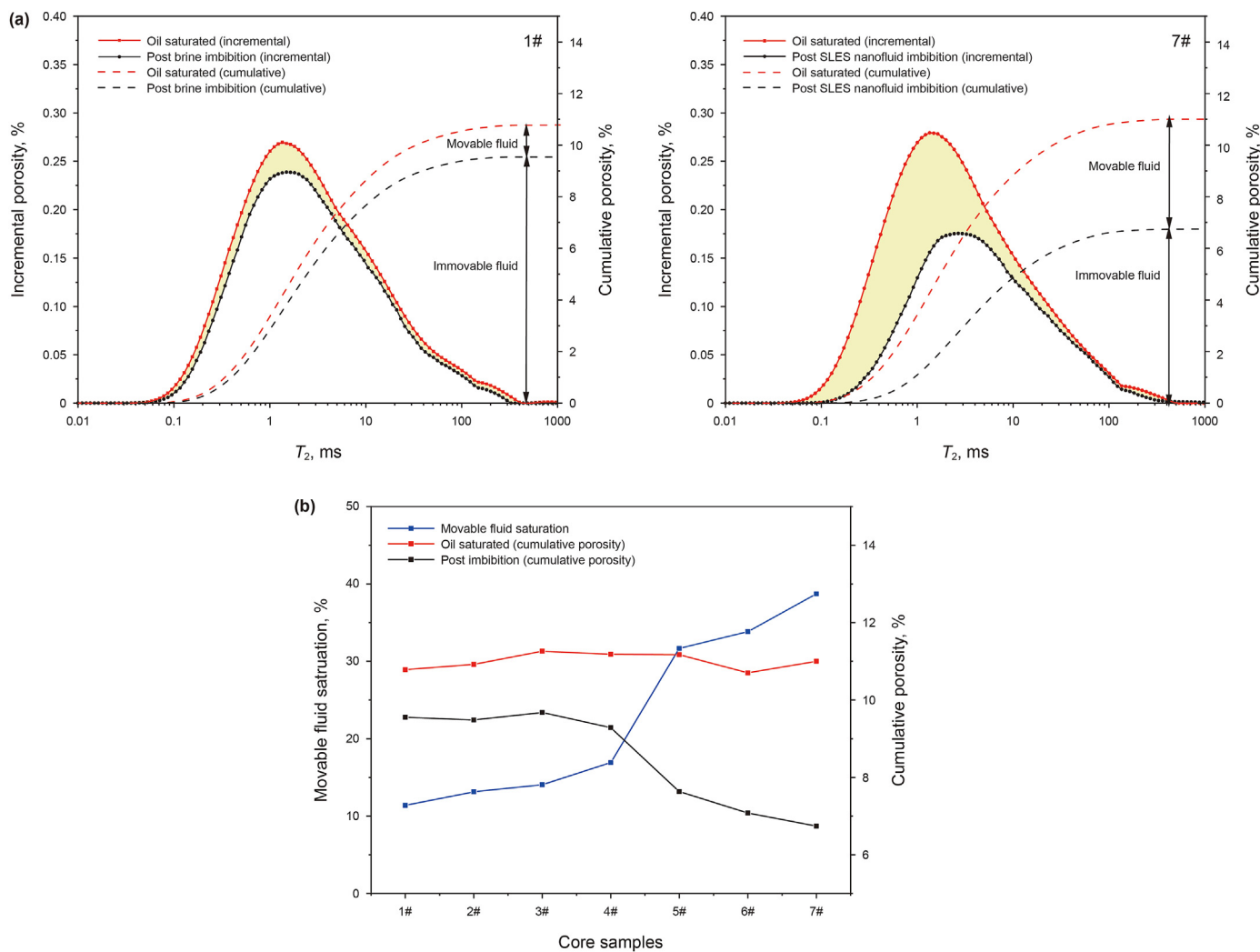

Fig. 13. (**a**) NMR incremental and cumulative spectra and (**b**) movable fluid saturation curve of sandstone core samples.

Table 4
Petrophysical properties and NMR analysis results of core samples.

| Sample No.	Imbibition fluid	Porosity, %	Permeability, mD	NMR porosity, %	Movable fluid porosity, %	NMR bound fluid saturation, %	NMR movable fluid saturation, %
1#	Brine	9.73	0.081	10.78	1.23	88.61	11.39
2#	Pure nanofluid	10.09	0.080	10.92	1.43	86.86	13.14
3#	DTAB nanofluid	9.81	0.088	11.26	1.58	85.94	14.06
4#	LHSB nanofluid	10.19	0.079	11.18	1.89	83.08	17.39
5#	APG12 nanofluid	10.70	0.078	11.17	3.54	68.34	32.36
6#	SDS nanofluid	10.99	0.073	10.70	3.62	65.72	34.28
7#	SLES nanofluid	11.26	0.072	10.99	4.26	61.03	38.97
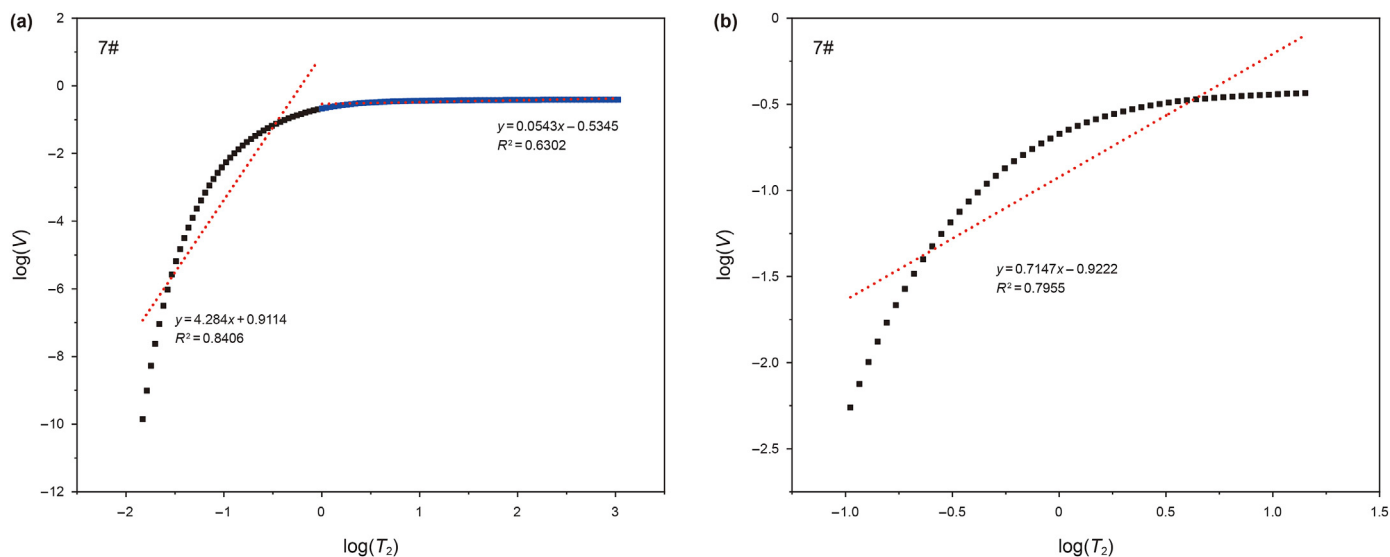
Fig. 14. NMR fractal characteristic curves of (**a**) overall and (**b**) movable fluid pores in sandstone core samples.

Table 5
NMR fractal dimension results of core samples.

Sample No.	$T_2 < 1$ ms		$T_2 > 1$ ms		Effective porosity	
	D_1	R^2	D_2	R^2	D	R^2
1#	−1.0553	0.8142	2.8975	0.8340	2.3739	0.8482
2#	−1.1576	0.8216	2.9406	0.7201	2.3642	0.8110
3#	−1.2253	0.8320	2.9082	0.8387	2.3609	0.8050
4#	−1.0457	0.8208	2.9128	0.8117	2.3591	0.8184
5#	−1.2951	0.8314	2.9313	0.7726	2.3213	0.7937
6#	−1.2349	0.8373	2.9135	0.7966	2.3188	0.8012
7#	−1.2843	0.8406	2.9457	0.6302	2.2853	0.7955

respectively. The NMR fractal dimensions of sandstone core samples are listed in Table 5. The fractal dimension D_1 ranged from −1.2867 to −1.0457 when T_2 was less than 1 ms, indicating that micropores did not have fractal characteristics. Meanwhile, the fractal dimension D_2 was in the range of 2.8975−2.9457 when T_2 was larger than 1 ms. This showed that the larger pores have fractal characteristics, and with strong heterogeneity and complexity. However, the overall fractal dimensions cannot favorably reflect the influence of nanofluids on the pore structure during the imbibition process (Zhou et al., 2019; Mao et al., 2020).

To effectively evaluate the influence of nanofluids on movable fluids, the fractal dimensions (D) of effective pores occupied with movable fluid (yellow part in Fig. 13(a) were calculated by Eq. (9). From Fig. 14(b) and Table 5, the fractal dimension D was in the range of 2.2853−2.3739 with an average value of 2.3405. The corresponding R^2 ranged from 0.7937 to 0.8482 with an average value

of 0.8104. The fractal dimension of movable fluid pores showed moderate complexity and heterogeneity of sandstone pore structures. It was observed from a combination of results of movable fluid and fractal dimension that fractal dimension D decreased and movable fluid saturation increased when nanofluids were used as imbibition agents. Particularly, SLES and SDS nanofluids exhibited superior performances including effective reduction in NMR bound fluid saturation and increment in NMR movable fluid saturation. Movable fluid occurred in pores less than 10 μm, and the complexity of pore structure determined the mobility of fluid in the sandstone core samples. The smaller the fractal dimension (D), the better the pore connectivity of core samples, resulting in a higher movable fluid saturation. Based on these analyses it can be concluded that, nanofluid can effectively lower pore complexity, causing a more homogeneous sandstone reservoir and also decrease the corresponding fractal dimension. This is more conducive to the storage and flow of movable fluids.

3.4. Spontaneous imbibition

To examine the potential performance of EOR using the proposed nanofluids, spontaneous imbibition tests of tight sandstone cores were conducted at 60 °C using 3 wt% brine, 0.05 wt% pure nanofluid, 0.05 wt% functional nanofluids, and 0.1 wt% pure surfactants, respectively. The oil imbibition recovery and imbibition rate were monitored to determine the efficiencies of the nanofluids as EOR agents. The spontaneous imbibition results are shown in Fig. 15(a and b) and Table 6. It was observed that the active nanofluids, especially SLES nanofluid, had an excellent performance in
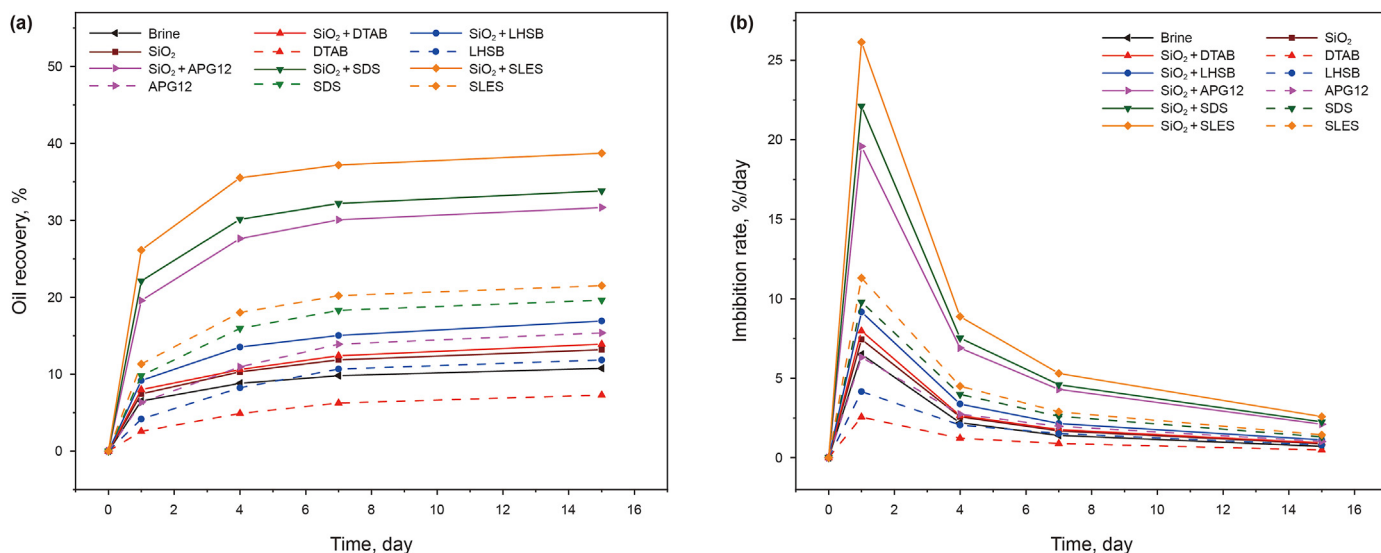
Fig. 15. Spontaneous imbibition results for brine, surfactants, and nanofluids: (**a**) oil imbibition recoverys versus time, (**b**) imbibition rate versus time.

Table 6
Imbibition results with different imbibition fluids.

Imbibition fluid	Imbibition recovery, %	Imbibition fluid	Imbibition recovery, %
3 wt% brine	10.75	0.05 wt% SiO_2	13.18
0.1 wt% DTAB	7.28	0.05 wt% SiO_2 + 0.1 wt% DTAB	13.90
0.1 wt% LHSB	11.85	0.05 wt% SiO_2 + 0.1 wt% LHSB	16.92
0.1 wt% APG12	15.36	0.05 wt% SiO_2 + 0.1 wt% APG12	31.66
0.1 wt% SDS	19.63	0.05 wt% SiO_2 + 0.1 wt% SDS	33.83
0.1 wt% SLES	21.51	0.05 wt% SiO_2 + 0.1 wt% SLES	38.71

terms of oil displacement than other imbibition fluids. Comparing the oil displacement performance with the brine, pure SiO_2 nanofluid and SLES, SLES nanofluid improved imbibition efficiencies by 27.96%, 25.53% and 17.20%, respectively. SDS and APG12 nanofluids also had good performance, with an imbibition recovery of 33.83% and 31.66%, respectively. However, the cationic DTAB and amphoteric LHSB nanofluids recovered only 13.90% and 16.92%, respectively. This means the cationic and amphoteric nanofluids had poor applicability in tight reservoirs. Fig. 15(b) shows that the imbibition rates increased rapidly at the beginning of the imbibition process. When the maximum imbibition rates were reached, the trend began to decrease, and finally reached zero. Additionally, it was found that the oil displacement rates of SLES and SDS nanofluids were much higher than other imbibition fluids. The imbibition results illustrated that the imbibition potential of fluids in tight sandstone was: SiO_2 + SLES > SiO_2 + SDS > SiO_2 + APG12 > SLES > SDS > SiO_2 + LHSB > SiO_2 + DTAB > SiO_2 > brine. Thus, the SDS and SLES nanofluids are suggested as potential EOR agents in tight oil reservoirs.

Moreover, Fig. 16(a) plots the T_2 spectra of oil phase in the cores at different imbibition stages (1# and 7#). From Fig. 16(a), the signal amplitude reduced when T_2 relaxation time was between 0.1 and 100 ms during imbibition. The signal amplitude hardly changed and the amount of oil in the cores no longer reduced until the end of imbibition. In addition, the T_2 spectrum of core 1# (immersed in brine) showed that the effect of brine imbibition was weak, with only a few droplets of oil produced. Compared with brine, the signal amplitude of the core immersed in 0.05 wt% SLES nanofluid significantly reduced. The oil in the micropores and mesopores of the rock core was initially mobilized, and the SLES nanofluid continuously entered the micropores and mesopores under the

action of capillary force, driving the oil into macropores, and then the oil was expelled from the core simultaneously. This is the main reason for the shift of the peaks of the NMR curves to the right (Zhou et al., 2019). Fig. 16(b) shows the contribution rate of oil recovery from different pores under different imbibition fluids. From Fig. 16(b), it was observed that the oil recovery contribution rate of micropores, mesopores and macropores of cores treated with different nanofluids were in the range of 4.52%–15.95%, 4.42%–17.01%, 1.53%–5.86%, respectively. This showed that mesopores and micropores contributed more to oil recovery than macropores. Based on these analyses it can be concluded that, nanofluid significantly improved the oil efficiency of tight sandstone cores due to their excellent properties.

3.5. EOR mechanism of functional nanofluid

The primary goal of this study is to understand the mechanisms involved in oil recovery from porous rocks using nanofluids. Combining the results of NMR and imbibition tests as well as interfacial properties of nanofluids, the underlying EOR mechanism of nanofluids can be summarized into three aspects: IFT reduction, wettability alteration and the structural disjoining pressure.

3.5.1. IFT reduction

The co-adsorption of silica nanoparticles and surfactant molecules evidently reduced the interfacial energy of the system, resulting in lower interfacial tension. In fact, there is no definite positive or negative correlation between the final oil recoveries and IFTs (Xu et al., 2021a). LHSB and DTAB nanofluids with lower IFTs (<2 mN/m), only improved the final oil recovery by 3.15% and 6.17% than that of brine, respectively. The primary cause of this
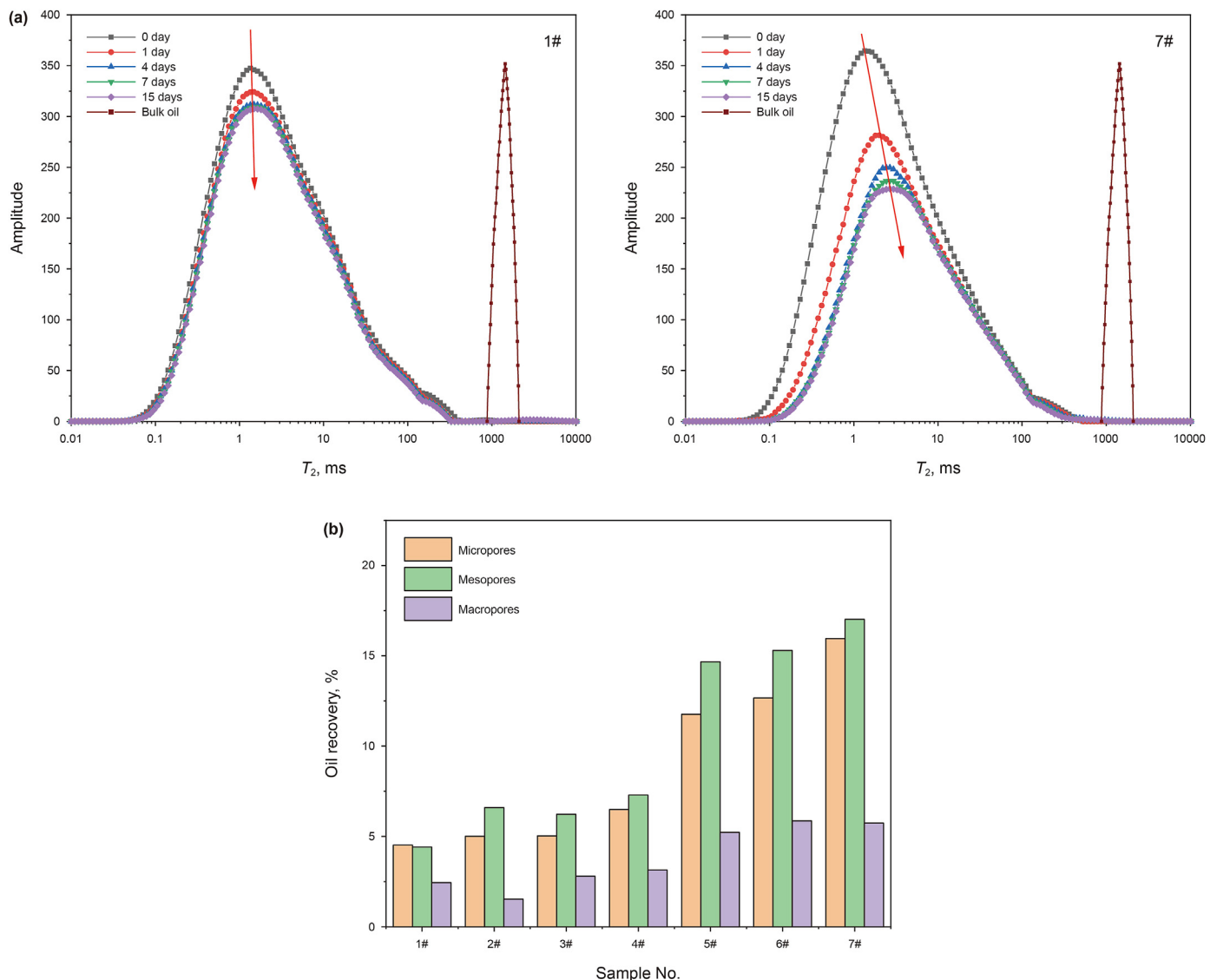
Fig. 16. (**a**) T_2 spectra during imbibition process of core immersed in 3 wt % brine and 0.05 wt% nanofluid, respectively. (**b**) The contribution rate of oil recovery from different pores under different imbibition fluids.

observation was the very low capillary pressure which could not provide the required driving force for spontaneous imbibition. However, SDS and SLES nanofluids with relatively higher IFTs (5−10 mN/m) had oil imbibition recovery of 33.83% and 38.71%, respectively. These two nanofluids decreased the adhesion between the oil and the rock surface, reducing the residual oil saturation from 88.61% to 61.29%. Besides, the oil droplets deformed under the action of the interfacial tension, and then passed through the smaller pore throat. This caused the oil to easily detach from the rock surface, and resulted in higher imbibition recovery. Thus, it is critical to seek a compromise of interfacial tension. An appropriate IFT reduction is needed to have a conducive oil detachment. Interestingly, APG12 nanofluid had lower IFT but performed well in terms of imbibition efficiency. This is expected because wettability alteration of nanofluids plays a considerable role in EOR (Kuang et al., 2018).

3.5.2. Wettability alteration

The effect of functional nanofluids on rock surface wettability is greater than that on interfacial tension. The contact angle results showed the ability of nanofluids to increase the water-wetness and this was in the order of SLES > SDS > APG12 > LHSB > DTAB > pure SiO_2 > brine. According to the formula of capillarity ($P_c = 2\sigma \cos \theta / r$), the capillary force as the driving force increased gradually with water-wetness. Compared with IFT reduction, wettability alteration was considered as a major factor for spontaneous imbibition, owing to the reversal of the capillary force caused by water-wetness. This is the reason why APG12 with lower IFT had higher imbibition recovery.

In addition, the pores wetted by nanofluids can be directly evaluated *in-situ* by comparing the measured oil recovery corresponding to the different pore types. Herein, the imbibition agent, SLES nanofluid was taken as an example. Based on the imbibition results, the measured oil recoveries corresponding to the micropores, mesopores, and macropores in the sandstone core immersed with SLES nanofluid increased from 4.52%, 4.42% and 2.45%− 15.95%, 17.01%, and 5.74%, respectively. This indicates micropores and mesopores played a vital role in the wetting process of the sandstone cores. These results can be explained by the pore properties and NMR results (Mao et al., 2020).
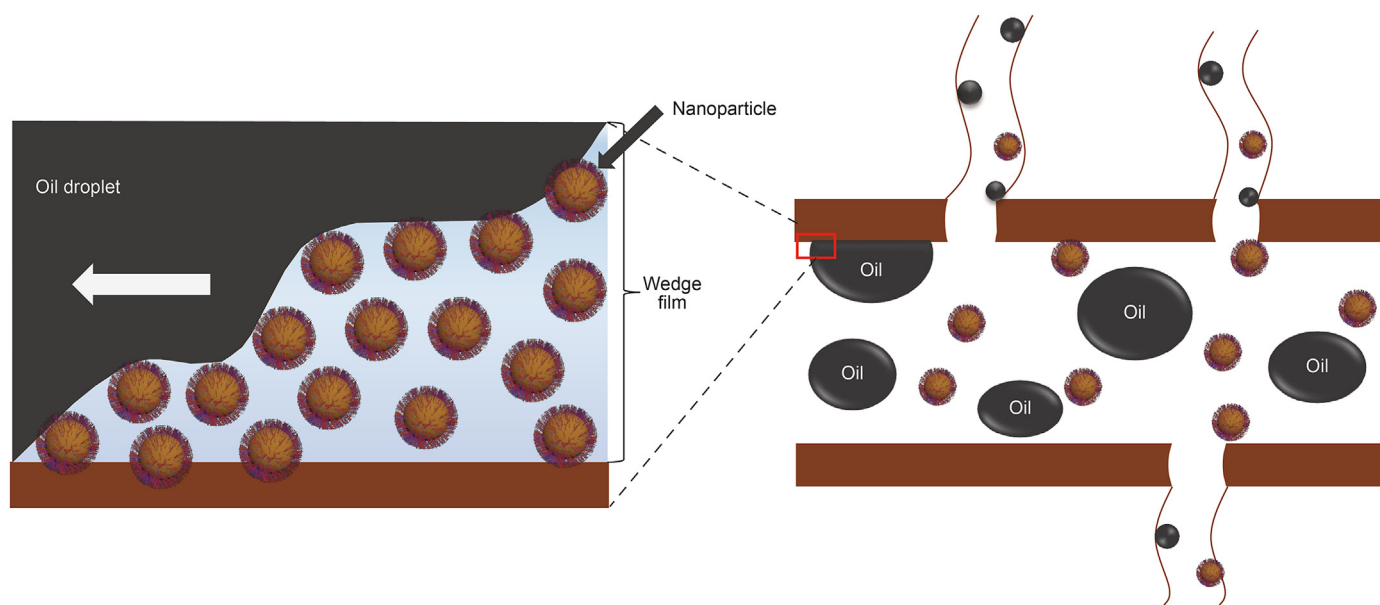
Fig. 17. Underlying EOR mechanism of the nanofluid.

The wettability of a reservoir controls the distribution of oil and water, as well as the movement of fluid through the pore space. The NMR surface relaxation is sensitive to the wettability of rocks (Zhou et al., 2019; Xu et al., 2022; Al-Garadi et al., 2022). From Fig. 16(a), it was observed that the crude oil in the core clearly shifted to shorter relaxation times compared to that of the bulk crude oil. This was due to the surface relaxation effects of crude oil. The crude oil in the pores of the rock interacted with the rock surface, making the rock surface lipophilic. In addition, as the SLES nanofluid imbibed into the rock cores, the dominant peak had a significant reduction and shifted to longer relaxation times. This behavior demonstrated a change in wettability. The T_2 relaxation times of dominant peaks approached that of the crude oil, showing that the oil droplets peeled off from the rock surface, and the surface relaxation effect was weakened. The rock surface was treated with SLES nanofluid, altering the wettability of the rock form oil wetness to water wetness. Unlike the SLES nanofluid, the above-mentioned phenomenon was not observed in the T_2 spectrum of core 7# which was immersed in 3 wt% brine. From Fig. 16(a), the T_2 relaxation time of maximum peak hardly shifted. After 4 days of brine imbibition, the T_2 spectrum no longer reduced. During the process imbibition, the oil and brine in the pores were redistributed without resulting in the shift of T_2 spectrum. This revealed that the wettability of rock surface was still oil-wet (Zhou et al., 2019). This was consistent with the results from contact angle tests.

3.5.3. Structural disjoining pressure

The co-adsorption of silica nanoparticles and surfactant molecules confined in oil/water/solid three-phase contact region was responsible for the EOR mechanism (Kuang et al., 2018). In the case of sandstones, the functional nanoparticles generated a wedge film between the oil and the rock surface, and a strong driving force existed within oil-water-solid three phase region, as seen in Fig. 17. During nanofluid imbibition into the rock core, the residual oil phases on the pore wall were separated from the rock surface by the structural disjoining pressure. The wettability of the pore throat became more water wet, reducing the adhesive force between the crude oil and the rock surface. This caused the oil droplets that were peeled off to no longer adsorb readily on the rock surface. The oil droplets were then displaced along with the migration of

nanofluids in the core pores. Thus, the adsorption behavior of nanofluids in the oil-water-solid three-phase region played a decisive role in spontaneous imbibition.

4. Conclusions

In this work, several nanofluids modified by different types of surfactants were prepared, and NMR technique was utilized to evaluate nanofluids for EOR applications in tight oil reservoirs. The following conclusions can be drawn from the study:

(1) The functional silica nanoparticles can be easily dispersed in DI water, and exhibited superior interface activity including IFT reduction and wettability alteration. Particularly, anionic-nonionic SLES nanofluids increased the most water-wetness in tight oil reservoirs.
(2) The tight sandstone pore system was categorized into micropores (<0.1 μm), mesopores (0.1–1 μm) and macropores (>1 μm). The mesopores were the dominant pore types, and were in the range of 50.54%–52.12%. The oil recovery contribution of micropores, mesopores and macropores were 4.52%–15.95%, 4.42%–17.01%, 1.53%–5.86%, respectively.
(3) SLES and SDS nanofluids had better EOR performance in tight oil reservoirs than other surfactant nanofluids. These two nanofluids were able to significantly reduce the residual oil saturation and increase crude oil mobility in the core pores. The imbibition mechanism of nanofluids in the tight oil reservoir was mainly IFT reduction, wettability alteration and structural disjoining pressure.

References

Adenutsi, C., Li, Z., Lai, F., et al., 2019. Pore pressure variation at constant confining

stress on water–oil and silica nanofluid–oil relative permeability. J. Pet. Explor. Prod. Technol. 9 (3), 2065–2079. https://doi.org/10.1007/s13202-018-0605-6.

Afekare, D., Gupta, I., Rao, D., 2020. Nanoscale investigation of silicon dioxide nanofluids and implications for enhanced oil recovery–An atomic force microscope study. J. Petrol. Sci. Eng. 191, 107165. https://doi.org/10.1016/j.petrol.2020.107165.

Afra, M., Peyghambarzadeh, S., Shahbazi, K., et al., 2021. Thermo-economic optimization of steam injection operation in enhanced oil recovery (EOR) using nano-thermal insulation. Energy 226, 120409. https://doi.org/10.1016/j.energy.2021.120409.

Al-Anssari, S., Barifcani, A., Wang, S., et al., 2016. Wettability alteration of oil-wet carbonate by silica nanofluid. J. Colloid Interface Sci. 461, 435–442. https://doi.org/10.1016/j.jcis.2015.09.051.

Al-Garadi, K., El-Husseiny, A., Elsayed, M., et al., 2022. A rock core wettability index using NMR T_2 measurements. J. Petrol. Sci. Eng. 208, 109386. https://doi.org/10.1016/j.petrol.2021.109386.

Chaturvedi, K.R., Sharma, T., 2020. Carbonated polymeric nanofluids for enhanced oil recovery from sandstone reservoir. J. Petrol. Sci. Eng. 194, 107499. https://doi.org/10.1016/j.petrol.2020.107499.

Chen, J.H., Zhang, H., Althaus, S.M., et al., 2021. High-spatial-resolution nuclear-magnetic-resonance method for investigation of fluid distribution in whole cores. Fuel 297, 120777. https://doi.org/10.1016/j.fuel.2021.120777.

Dai, C., Cheng, R., Sun, X., et al., 2019. Oil migration in nanometer to micrometer sized pores of tight oil sandstone during dynamic surfactant imbibition with online NMR. Fuel 245, 544–553. https://doi.org/10.1016/j.fuel.2019.01.021.

Hassan, Y., Guan, H., Chuan, L., et al., 2022. Interfacial tension and wettability of hybridized $ZnOFe_2O_3/SiO_2$ based nanofluid under electromagnetic field inducement. J. Petrol. Sci. Eng., 110184 https://doi.org/10.1016/j.petrol.2022.110184.

Jafarbeigi, E., Salimi, F., Kamari, E., et al., 2021. Effects of modified GO nano-fluid on wettability and IFT changes: experimental study for EOR applications. Petrol. Sci. https://doi.org/10.1016/j.petsci.2021.12.022.

Jiang, L., Li, S., Yu, W., et al., 2016. Interfacial study on the interaction between hydrophobic nanoparticles and ionic surfactants. Colloid. Surface. 488, 20–27. https://doi.org/10.1016/j.colsurfa.2015.10.007.

Kathel, P., Mohanty, K., 2018. Dynamic surfactant-aided imbibition in fractured oil-wet carbonates. J. Petrol. Sci. Eng. 170, 898–910. https://doi.org/10.1016/j.petrol.2018.06.088.

Kuang, W., Saraji, S., Piri, M., 2018. A systematic experimental investigation on the synergistic effects of aqueous nanofluids on interfacial properties and their implications for enhanced oil recovery. Fuel 220, 849–870. https://doi.org/10.1016/j.fuel.2018.01.102.

Li, Y., Dai, C., Zhou, H., et al., 2017. A novel nanofluid based on fluorescent carbon nanoparticles for enhanced oil recovery. Ind. Eng. Chem. Res. 56 (44), 12464–12470. https://doi.org/10.1021/acs.iecr.7b03617.

Li, Y., Dai, C., Zhou, H., et al., 2018a. Investigation of spontaneous imbibition by using a surfactant-free active silica water-based nanofluid for enhanced oil recovery. Energy Fuel. 32 (1), 287–293. https://doi.org/10.1021/acs.energyfuels.7b03132.

Li, Z., Shen, X., Qi, Z., et al., 2018b. Study on the pore structure and fractal characteristics of marine and continental shale based on mercury porosimetry, N_2 adsorption and NMR methods. J. Nat. Gas Sci. Eng. 53, 12–21. https://doi.org/10.1016/j.jngse.2022.02.027.

Liang, T., Hou, J., Qu, M., et al., 2021a. Application of nanomaterial for enhanced oil recovery. Petrol. Sci. https://doi.org/10.1016/j.petsci.2021.11.011.

Liang, T., Hou, J., Xi, J., 2021b. Mechanisms of nanofluid based modification MoS_2 nanosheet for enhanced oil recovery in terms of interfacial tension, wettability alteration and emulsion stability. J. Dispersion Sci. Technol. 1–12. https://doi.org/10.1080/01932691.2021.1930034.

Liu, J., Sheng, J.J., Wang, X., et al., 2019. Experimental study of wettability alteration and spontaneous imbibition in Chinese shale oil reservoirs using anionic and nonionic surfactants. J. Petrol. Sci. Eng. 175, 624–633. https://doi.org/10.1016/j.petrol.2019.01.003.

Liu, W., Wang, G., Han, D., et al., 2021. Accurate characterization of coal pore and fissure structure based on CT 3D reconstruction and NMR. J. Nat. Gas Sci. Eng. 96, 104242. https://doi.org/10.1016/j.jngse.2021.104242.

Maghzi, A., Mohammadi, S., Ghazanfari, M.H., et al., 2012. Monitoring wettability alteration by silica nanoparticles during water flooding to heavy oils in five-spot systems: a pore-level investigation. Exp. Therm. Fluid Sci. 40, 168–176. https://doi.org/10.1016/j.expthermflusci.2012.03.004.

Mao, Y., Xia, W., Peng, Y., et al., 2020. Wetting of coal pores characterized by LF-NMR and its relationship to flotation recovery. Fuel 272, 117737. https://doi.org/10.1016/j.fuel.2020.117737.

Mousavi, S.B., Heris, S.Z., Estellé, P., 2021. Viscosity, tribological and physicochemical features of ZnO and MoS_2 diesel oil-based nanofluids: an experimental study. Fuel 293, 120481. https://doi.org/10.1016/j.fuel.2021.120481.

Nowrouzi, I., Manshad, A.K., Mohammadi, A.H., 2019. Effects of concentration and size of TiO_2 nano-particles on the performance of smart water in wettability alteration and oil production under spontaneous imbibition. J. Petrol. Sci. Eng. 183, 106357. https://doi.org/10.1016/j.petrol.2019.106357.

Nwidee, L.N., Lebedev, M., Barifcani, A., et al., 2017. Wettability alteration of oil-wet limestone using surfactant-nanoparticle formulation. J. Colloid Interface Sci. 504, 334–345. https://doi.org/10.1016/j.jcis.2017.04.078.

Qiu, Z., Zhou, Y., Yao, Y., et al., 2019. Modification of microencapsulated phase change materials (MPCMs) by synthesizing graphene quantum dots (GQDs) and nano-aluminum for energy storage and heat transfer applications. Energy 181, 1331–1338. https://doi.org/10.1016/j.energy.2019.05.080.

Sagala, F., Hethnawi, A., Nassar, N.N., 2020. Hydroxyl-functionalized silicate-based nanofluids for enhanced oil recovery. Fuel 269, 117462. https://doi.org/10.1016/j.fuel.2020.117462.

Sangeetha, M., Manigandan, S., Ashok, B., et al., 2021. Experimental investigation of nanofluid based photovoltaic thermal (PV/T) system for superior electrical efficiency and hydrogen production. Fuel 286, 119422. https://doi.org/10.1016/j.fuel.2020.119422.

Sentein, C., Guizard, B., Giraud, S., et al., 2009. Dispersion and stability of TiO_2 nanoparticles synthesized by laser pyrolysis in aqueous suspensions. In: J Phys : Conference Series. IOP Publishing, 012013. https://doi:10.1088/1742-6596/170/1/012013.

Shalbafan, M., Esmaeilzadeh, F., Safaei, A., 2019. Experimental investigation of wettability alteration and oil recovery enhance in carbonate reservoirs using iron oxide nanoparticles coated with EDTA or SLS. J. Petrol. Sci. Eng. 180, 559–568. https://doi.org/10.1016/j.petrol.2019.05.085.

Su, S., Jiang, Z., Shan, X., et al., 2018. The wettability of shale by NMR measurements and its controlling factors. J. Petrol. Sci. Eng. 169, 309–316. https://doi.org/10.1016/j.petrol.2018.05.067.

Sun, Y., Zhai, C., Xu, J., et al., 2020. A method for accurate characterisation of the pore structure of a coal mass based on two-dimensional nuclear magnetic resonance T_1-T_2. Fuel 262, 116574. https://doi.org/10.1016/j.fuel.2019.116574.

Wang, F., Zeng, F., Wang, L., et al., 2021a. Fractal analysis of tight sandstone petrophysical properties in unconventional oil reservoirs with NMR and rate-controlled porosimetry. Energy Fuel. 35 (5), 3753–3765. https://doi.org/10.1021/acs.energyfuels.0c03394.

Wang, Z., Zhao, H., Zhang, Y., et al., 2021b. Surfactant-guided spatial assembly of nano-architectures for molecular profiling of extracellular vesicles. Nat. Commun. 12 (1), 1–12. https://doi.org/10.1038/s41467-021-23759-9.

Wuebbeler, G., Marschall, M., Rühl, E., et al., 2021. Compressive nano-FTIR chemical mapping. Meas. Sci. Technol. https://doi.org/10.1088/1361-6501/ac407a.

Xu, D., Li, Z., Bai, B., et al., 2021a. A systematic research on spontaneous imbibition of surfactant solutions for low permeability sandstone reservoirs. J. Petrol. Sci. Eng., 109003 https://doi.org/10.1016/j.petrol.2021.109003.

Xu, R., Yang, S., Xiao, Z., et al., 2022. Quantitatively study on imbibition of fracturing fluid in tight sandstone reservoir under high temperature and high pressure based on NMR technology. J. Petrol. Sci. Eng. 208, 109623. https://doi.org/10.1016/j.petrol.2021.109623.

Xu, Y., Zheng, H., Schumacher, D., et al., 2021b. Recent advancements of specific functionalized surfaces of magnetic nano-and microparticles as a theranostics source in biomedicine. ACS Biomater. Sci. Eng. https://doi.org/10.1021/acsbiomaterials.0c01393.

Yuan, Y., Rezaee, R., 2019. Fractal analysis of the pore structure for clay bound water and potential gas storage in shales based on NMR and N_2 gas adsorption. J. Petrol. Sci. Eng. 177, 756–765. https://doi.org/10.1016/j.petrol.2019.02.082.

Zadeh, S.M.H., Mehryan, S., Ghalambaz, M., et al., 2020. Hybrid thermal performance enhancement of a circular latent heat storage system by utilizing partially filled copper foam and Cu/GO nano-additives. Energy 213, 118761. https://doi.org/10.1016/j.energy.2020.118761.

Zhang, C., Zeng, Z., Cui, D., et al., 2021a. Semiconducting polymer nano-PROTACs for activatable photo-immunometabolic cancer therapy. Nat. Commun. 12 (1), 1–12. https://doi.org/10.1038/s41467-021-23194-w.

Zhang, T., Zou, Q., Cheng, Z., et al., 2021b. Effect of particle concentration on the stability of water-based SiO_2 nanofluid. Powder Technol. 379, 457–465. https://doi.org/10.1016/j.powtec.2020.10.073.

Zhang, T., Zou, Q., Jia, X., et al., 2022. Effect of cyclic water injection on the wettability of coal with different SiO_2 nanofluid treatment time. Fuel 312, 122922. https://doi.org/10.1016/j.fuel.2021.122922.

Zhao, Y., Wang, C., Ning, L., et al., 2022. Pore and fracture development in coal under stress conditions based on nuclear magnetic resonance and fractal theory. Fuel 309, 122112. https://doi.org/10.1016/j.fuel.2021.122112.

Zhou, H., Zhang, Q., Dai, C., et al., 2019. Experimental investigation of spontaneous imbibition process of nanofluid in ultralow permeable reservoir with nuclear magnetic resonance. Chem. Eng. Sci. 201, 212–221. https://doi.org/10.1016/j.ces.2019.02.036.

Zhou, Y., Wu, X., Zhong, X., et al., 2020. Polymer nanoparticles based nano-fluid for enhanced oil recovery at harsh formation conditions. Fuel 267, 117251. https://doi.org/10.1016/j.fuel.2020.117251.